International Journal of Heat and Mass Transfer 52 (2009) 1206–1213

Contents lists available at ScienceDirect

International Journal of Heat and Mass Transfer

journal homepage: www.elsevier.com/locate/ijhmt

Thermal lagging in multi-carrier systems

Da Yu Tzou [a,*], Weizhong Dai [b]

[a] Department of Mechanical and Aerospace Engineering, University of Missouri, Columbia, MO 65211, USA
[b] Mathematics and Statistics, College of Engineering and Science, Louisiana Tech University, Ruston, LA 71272, USA

ARTICLE INFO

Article history:
Received 3 March 2008
Received in revised form 18 August 2008
Available online 29 October 2008

Keywords:
Nonequilibrium heating
Energy exchange
Multi-carrier systems
Thermal lagging
Microscale

ABSTRACT

Nonequilibrium heating in multi-carrier systems is captured by the high-order effects in thermal lagging. Following the general formulation for the *N*-carrier system, a three-carrier system follows, aiming toward extracting the intrinsic behavior of ultrafast thermalization and relaxation among different carriers. For the first time to our knowledge, it shows that energy coupling among three carriers gives rise to the new τ_T^2-effect, which also results in a flux-precedence type of heat flow. Nondimensional analysis is made to extract the dominating parameters, including the ratio between the two phase lags expressed in terms of two heat-capacity and two energy-coupling-factor ratios. In the numerical example, the method of Laplace transform is used to solve the heat equation with nonlinear effects of both τ_T^2 and τ_q^2. Thermal lagging with the additional effect of τ_T^2 further elevates the field temperature as compared to the τ_q^2-effect alone.

1. Introduction

Energy exchange between electrons and phonons in metals provides the best example in describing nonequilibrium heating during the ultrafast transient [1–6]. In times comparable to the thermalization and relaxation times of electrons and phonons, which are in the range from a few to several tens of picoseconds, heat continuously flows from hot electrons to cold phonons through mutual collisions. Consequently, electron temperature continuously decreases whereas phonon temperature continuously increases until thermal equilibrium is reached. Intensity of heat flow during nonequilibrium heating is proportional to the temperature difference between electrons and phonons. The proportional constant is termed electron–phonon coupling factor, which is a new thermophysical property in microscale heat transfer. The same concept has been extended to model pulsed heating on amorphous media [6] and nonequilibrium heat transport in porous media [7]. In place of electrons and phonons, energy coupling between the solid and fluid/gaseous phases was described in the same way. The thermalization and relaxation times for slow materials, such as lightly packed copper spheres or rough carbon surfaces [6,8], can reach several tenths of a millisecond due to the low-conducting phases involved in the assemblies. Transient times on the order of 10^{-4} s, therefore, are considered to be ultrafast because of the pronounced thermalization and relaxation behaviors observed in the sub-millisecond domain.

Nonequilibrium heating in porous media [7] already involves a more complicated system than the two-carrier (electron–phonon) system in metals. Phase change in wicked heat pipes, moreover, often involves nonequilibrium heating/energy dissipation among the solid wick, liquid, and vapor phases [9]. As extension is made to medical applications employing femtosecond lasers [10], complexities of nonequilibrium heating further evolves due to involvement of multiple carriers in biomedical systems, including hard/soft tissues (proteins), water, and minerals at least. The ways in which thermal energy is distributed among different carriers, as well as the characteristic times dictating the intrinsic behaviors of nonequilibrium heating, plays a dominant role in assuring the success of femtosecond-laser technologies.

This work generalizes the two-carrier system into the *N*-carrier system in describing the physical mechanisms of nonequilibrium heating. Particular emphasis will be placed on extracting the relaxation and thermalization times that characterize the lagging behavior during the ultrafast transition. For systems involving three carriers, specifically, harmonic decomposition is applied to obtain a single energy equation that unveils the intrinsic behavior of thermal lagging. In addition to the second-order effect in τ_q^2, thermal lagging in a three-carrier system gives rise to an additional effect of τ_T^2, rendering a flux-precedence type of heat flow that only existed in theory prior to the present analysis. A nondimensional analysis is performed to extract the dominating parameters during the ultrafast transient. The two phase lags, as well as their ratio, are derived and represented in terms of heat-capacity and energy-coupling-factor ratios.

2. *N*-Carrier system

Although thermophysical properties would be temperature dependent in general, particularly in complicated physical systems undergoing a wide temperature change, they will be assumed

* Corresponding author. Tel.: +1 573 882 4060; fax: +1 573 884 5090.
E-mail address: tzour@missouri.edu (D.Y. Tzou).

0017-9310/$ - see front matter © 2008 Elsevier Ltd. All rights reserved.
doi:10.1016/j.ijheatmasstransfer.2008.08.029

Nomenclature

C	volumetric heat capacity (J m^{-3} K^{-1})
G_i	energy coupling factor between carrier i and j (W m^{-3} K^{-1})
k	thermal conductivity (W m^{-1} K^{-1})
m	summation index
N	total number of carriers
p	parameter of Laplace transform
q	heat flux vector (W m^{-2})
T	temperature (K)

Greek symbols

β	nondimensional time
γ	real axis of Bromwich contour
θ	nondimensional temperature
τ	phase lag (s)
ξ	nondimensional space

Subscripts and superscripts

e	electrons
i	carrier i
l	lattices
q	heat flux
Re	real part
T	temperature
$\dot{X}$	$\partial X/\partial t$
$\bar{X}$	Laplace transform of X
∇^2	Laplacian

constant for the time being to characterize the fundamental behavior of energy transport. Fig. 1 shows the energy exchanges among dissimilar energy carriers, which are assumed proportional to their temperature differences as that assumed during electron–phonon coupling [1–5]. The energy equations governing the N carriers are

$$\begin{aligned} C_1\frac{\partial T_1}{\partial t} &= k_1\nabla^2 T_1 - \sum_{i=2}^{N} G_{1i}(T_1 - T_i);\\ C_m\frac{\partial T_m}{\partial t} &= k_m\nabla^2 T_m + \sum_{j=1}^{m-1} G_{jm}(T_j - T_m)\\ &\quad - \sum_{i=m+1}^{N} G_{mi}(T_m - T_i), \quad m = 2,3,\ldots,(N-1);\\ C_N\frac{\partial T_N}{\partial t} &= k_N\nabla^2 T_N + \sum_{i=1}^{N-1} G_{iN}(T_i - T_N). \end{aligned} \tag{1}$$

All N carriers are assumed stationary in the system. To describe the advection effects, all derivatives with respect to time on the left-hand side of Eq. (1) are replaced by the total derivatives. The summations with negative/positive signs in the front represent the energy loss/gain to/from other carriers. The first summation in the second expression, for example, represents the volumetric energy density received by carrier m, whereas the second summation in the same equation represents the energy density released from carrier m. Nonequilibrium heating is reflected by the temperature differences in Eq. (1). After thermalization where thermal equilibrium is achieved among N carriers, all G-terms in Eq. (1) diminish and Fourier diffusion is recovered.

Eq. (1) represents N coupled equations for N unknowns, which are to be solved for T_1 to T_N subject to the appropriate initial (N) and boundary ($2N$) conditions describing the physical system.

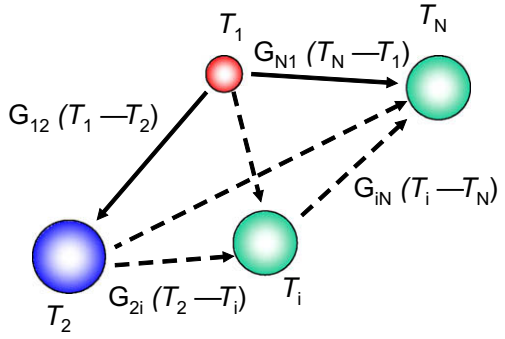

Fig. 1. Energy exchange in a system with N carriers.

The thermalization time at which $T_i = T_j$, with $i, j = 1,2,\ldots, N$ but $i \neq j$, is an obvious focus in deriving the solutions since it describes the finite time required for some/all carriers to achieve thermal equilibrium.

2.1. Three-carrier system

In the case of a two-carrier system, exemplified by metals with free electrons (e) and periodic lattices (l), the first and third equations in Eq. (1) reduce to

$$\begin{aligned} C_1\frac{\partial T_1}{\partial t} &= k_1\nabla^2 T_1 - G_{12}(T_1 - T_2);\\ C_2\frac{\partial T_2}{\partial t} &= k_2\nabla^2 T_2 + G_{12}(T_1 - T_2). \end{aligned} \tag{2}$$

Replacing "1" by "e" (for electrons) and "2" by "l" (for lattices), Eq. (2) reduces to the parabolic two-step heating model in microscale heat transfer [5]. Neglecting the effect of conduction in thin metal lattices, $k_2 \equiv k_l = 0$, Eq. (2) further reduces to the energy equation for a femtosecond-laser heated microfilm [3–6]. In passing, note that Eq. (2) can be combined to yield a single energy equation for either the electron (1) or lattice (2) temperature [5,6]:

$$\nabla^2 T + \left(\frac{C_2}{G_{12}}\right)\frac{\partial}{\partial t}(\nabla^2 T) = \left(\frac{C_1 + C_2}{k_1}\right)\frac{\partial T}{\partial t} + \left(\frac{C_1 C_2}{k_1 G_{12}}\right)\frac{\partial^2 T}{\partial t^2} \tag{3}$$

Both T_1 and T_2 are governed by the same equation, with the mixed-derivative term, $\partial(\nabla^2 T)/\partial t$ on the left-hand side, and the wave term, $\partial^2 T/\partial t^2$ on the right-hand side, describing the ultrafast thermalization and relaxation between electrons and lattices. Even though Eq. (2) bears the familiar appearance of Fourier diffusion, in other words, the energy coupling terms (led by G_{12}) result in the *thermalization time* (C_2/G_{12}) and the *relaxation time* ($C_1C_2/[G_{12}(C_1 + C_2)]$) that are two intrinsic time constants characterizing the ultrafast response in thin metal films.

Eq. (1) can be degenerated into a system with three carriers, i.e., $N = 3$. Examples include all composites with three constituents, interfacial heat transport involving two materials in contact and the interstitial gas, phase change in wicked heat pipes involving liquid, vapor and solid phase, on-chip bioprocesses involving separation of protein from water and minerals, and burned skin removal by femtosecond lasers that displays mixtures of healthy skins, burned tissues, and charring materials on the surface. The number of carriers involved in these systems could further evolve should nonequilibrium heating be tackled in each phase, such as electrons and phonons in the metallic solid phase. For systems involving three carriers, Eq. (1) reduces to

$$
\begin{aligned}
C_1\frac{\partial T_1}{\partial t} &= k_1\nabla^2 T_1 - G_{12}(T_1-T_2) - G_{13}(T_1-T_3);\\
C_2\frac{\partial T_2}{\partial t} &= k_2\nabla^2 T_2 + G_{12}(T_1-T_2) - G_{23}(T_2-T_3);\\
C_3\frac{\partial T_3}{\partial t} &= k_3\nabla^2 T_3 + G_{13}(T_1-T_3) + G_{23}(T_2-T_3).
\end{aligned}
\tag{4}
$$

There are efficient numerical algorithms solving this type of coupled differential equations [11]. The fundamental behavior characterizing the process of nonequilibrium heating, parallel the thermalization and relaxation times in Eq. (3) that characterize the two-carrier system, however, is what we are mainly concerned with in this work. The characteristic times defining nonequilibrium heating belong to the transient response, in time. For simplifying the elimination process, therefore, heat transport in a one-dimensional system will be assumed from now on to avoid unnecessary complications from the space operators. The Laplacian operator (∇^2) in Eq. (4), therefore, is replaced by $\partial^2/\partial x^2$.

2.2. Harmonic decomposition

Eq. (4) involves more than a simple Fourier diffusion as reflected in its first glance. To extract the characteristic times governing the energy exchange during nonequilibrium heating, we manage to eliminate two temperatures from the existing three unknowns T_1, T_2, and T_3. Eliminating two unknowns from them to render a single energy equation like Eq. (3), however, is not as straightforward as that in a two-carrier system [5,6]. A generic procedure is to introduce the harmonic analysis by assuming

$$
T_i(x,t) = \Gamma_i(t)\sin(n\pi x), \quad i = 1,2,3. \tag{5}
$$

Substituting Eq. (5) into Eq. (4), the coupled PDEs are reduced to coupled ODEs:

$$
\begin{aligned}
C_1\frac{d\Gamma_1}{dt} &= -(n^2\pi^2 k_1 + G_{12} + G_{13})\Gamma_1 + G_{12}\Gamma_2 + G_{13}\Gamma_3;\\
C_2\frac{d\Gamma_2}{dt} &= G_{12}\Gamma_1 - (n^2\pi^2 k_2 + G_{12} + G_{23})\Gamma_2 + G_{23}\Gamma_3;\\
C_3\frac{d\Gamma_3}{dt} &= G_{13}\Gamma_1 + G_{23}\Gamma_2 - (n^2\pi^2 k_3 + G_{13} + G_{23})\Gamma_3.
\end{aligned}
\tag{6}
$$

First, Γ_3 is expressed in terms of Γ_1, Γ_2, and $\dot{\Gamma}_2$ from the second expression in Eq. (6). Substituting the result into the remaining two equations in Eq. (6), it results in two equations (remained coupled) for two unknowns, Γ_1 and Γ_2. Both equations contain a common term of $\dot{\Gamma}_1$. Eliminating $\dot{\Gamma}_1$ from these two equations, second, Γ_1 can be expressed in terms of Γ_2, $\dot{\Gamma}_2$ and $\ddot{\Gamma}_2$. The resulting expression for Γ_1 can then be substituted into either one of the two equations (containing Γ_1 and Γ_2) for obtaining the single energy equation governing Γ_2. The result is

$$
\begin{aligned}
&(C_1C_2C_3)\frac{d^3\Gamma_2}{dt^3} + [C_2C_3(G_{12}+G_{13}) + C_1C_3(G_{12}+G_{23})\\
&\quad + C_1C_2(G_{13}+G_{23}) + (C_1C_2k_3 + C_2C_3k_1 + C_1C_3k_2)n^2\pi^2]\frac{d^2\Gamma_2}{dt^2}\\
&\quad + \{_{①}(C_1+C_2+C_3)(G_{13}G_{23}+G_{12}G_{13}+G_{12}G_{23})\\
&\quad + \{_{②}C_1[G_{13}k_2 + G_{12}k_3 + G_{23}(k_2+k_3)]\\
&\quad + C_2[G_{23}k_1 + G_{12}k_3 + G_{13}(k_1+k_3)]\\
&\quad + C_3[G_{23}k_1 + G_{13}k_2 + G_{12}(k_1+k_2)]\}_{②}(n\pi)^2\\
&\quad + (C_1k_2k_3 + C_2k_1k_3 + C_3k_1k_2)(n\pi)^4\}_{①}\frac{d\Gamma_2}{dt}\\
&\quad + \{_{③}(k_1+k_2+k_3)[G_{13}G_{23}+G_{12}G_{13}+G_{12}G_{23}](n\pi)^2\\
&\quad + [G_{12}k_3(k_1+k_2) + G_{13}k_2(k_1+k_3) + G_{23}k_1(k_2+k_3)](n\pi)^4\\
&\quad + k_1k_2k_3(n\pi)^6\}_{③}\Gamma_2 = 0
\end{aligned}
\tag{7}
$$

where the paired parentheses are labeled for easier recognition. Multiplying Eq. (7) throughout by $\sin(n\pi x)$ and recovering the partial derivatives in accordance with Eq. (5),

$$
\begin{aligned}
&\frac{\partial^6 T_2}{\partial x^6} = -(n\pi)^6\Gamma_2(t)sin(n\pi x), \quad \frac{\partial^4 T_2}{\partial x^4} = (n\pi)^4\Gamma_2(t)sin(n\pi x);\\
&\frac{\partial^2 T_2}{\partial x^2} = -(n\pi)^2\Gamma_2(t)sin(n\pi x), \quad \frac{\partial^5 T_2}{\partial x^4\partial t} = (n\pi)^4\dot{\Gamma}_2(t)sin(n\pi x);\\
&\frac{\partial^4 T_2}{\partial x^2\partial t^2} = -(n\pi)^2\ddot{\Gamma}_2(t)sin(n\pi x), \quad \frac{\partial^3 T_2}{\partial x^2\partial t} = -(n\pi)^2\dot{\Gamma}_2(t)sin(n\pi x);\\
&\frac{\partial T_2}{\partial t} = \dot{\Gamma}_2(t)sin(n\pi x), \quad \frac{\partial^2 T_2}{\partial t^2} = \ddot{\Gamma}_2(t)sin(n\pi x), \quad \frac{\partial^3 T_2}{\partial t^3} = \dddot{\Gamma}_2(t)sin(n\pi x),
\end{aligned}
\tag{8}
$$

The single energy equation governing T_2 is

$$
\begin{aligned}
&(C_1C_2C_3)\frac{\partial^3 T_2}{\partial t^3} + [C_2C_3(G_{12}+G_{13}) + C_1C_3(G_{12}+G_{23})\\
&\quad + C_1C_2(G_{13}+G_{23})]\frac{\partial^2 T_2}{\partial t^2}\\
&\quad + (C_1+C_2+C_3)(G_{13}G_{23}+G_{12}G_{13}+G_{12}G_{23})\frac{\partial T_2}{\partial t}\\
&= (k_1+k_2+k_3)[G_{13}G_{23}+G_{12}G_{13}+G_{12}G_{23}]\frac{\partial^2 T_2}{\partial x^2}\\
&\quad - [G_{12}k_3(k_1+k_2) + G_{13}k_2(k_1+k_3) + G_{23}k_1(k_2+k_3)]\frac{\partial^4 T_2}{\partial x^4}\\
&\quad + (k_1k_2k_3)\frac{\partial^6 T_2}{\partial x^6} + \{C_1[G_{13}k_2 + G_{12}k_3 + G_{23}(k_2+k_3)]\\
&\quad + C_2[G_{23}k_1 + G_{12}k_3 + G_{13}(k_1+k_3)] + C_3[G_{23}k_1 + G_{13}k_2\\
&\quad + G_{12}(k_1+k_2)]\}\frac{\partial^3 T_2}{\partial x^2\partial t} + (C_1C_2k_3 + C_2C_3k_1 + C_1C_3k_2)\frac{\partial^4 T_2}{\partial x^2\partial t^2}\\
&\quad -(C_1k_2k_3 + C_2k_1k_3 + C_3k_1k_2)\frac{\partial^5 T_2}{\partial x^4\partial t}
\end{aligned}
\tag{9}
$$

The same procedure can be applied to yield a single energy equation for T_1 or T_3. They have exactly the same form as Eq. (9) due to symmetry in exchanging thermal energy. Buried in the coupled diffusion equations shown by Eq. (4), clearly, heat transport in each carrier involves *anomalous* diffusion containing numerous high-order effects in space. The sixth-order derivative results from three second-order derivatives in Eq. (4). The mixed-derivative terms with respect to both space (x) and time (t), most important, may imply the characteristic times that define the transient response. Harmonic decomposition used here to eliminate multiple temperatures (T_1 and T_3) from the coupled PDEs (Eq. (4)) emphasizes the sinusoidal responses of temperatures in space (Eq. (5)). A recent work employed the direct operator method for elimination [12], which results in the same expression for T_2 as shown in Eq. (9).

To extract the characteristic times governing the fast transient described by Eq. (9), we assume carrier 1 and carrier 3 are so small that effect of conduction is negligible in them. This is the same assumption as that of the thin metal lattices made in the microscopic two-step model [3–6]. Mathematically, k_1 and k_3 are set to zero in Eq. (4). Eq. (9) then becomes

$$
\begin{aligned}
&\frac{\partial^2 T_2}{\partial x^2} + D_{21}\frac{\partial^3 T_2}{\partial t\partial x^2} + D_{22}\frac{\partial^4 T_2}{\partial t^2\partial x^2} = D_1\frac{\partial T_2}{\partial t}\\
&\quad + D_2\frac{\partial^2 T_2}{\partial t^2} + D_3\frac{\partial^3 T_2}{\partial t^3}
\end{aligned}
$$

where

$$D_{21}=\frac{C_1(G_{13}+G_{23})+C_3(G_{12}+G_{13})}{G_{13}G_{23}+G_{12}G_{13}+G_{12}G_{23}},$$
$$D_{22}=\frac{C_1C_3}{G_{13}G_{23}+G_{12}G_{13}+G_{12}G_{23}},$$
$$D_1=\frac{C_1+C_2+C_3}{k_2},$$
$$D_2=\frac{C_1C_2(G_{13}+G_{23})+C_1C_3(G_{12}+G_{23})+C_2C_3(G_{12}+G_{13})}{k_2(G_{13}G_{23}+G_{12}G_{13}+G_{12}G_{23})},$$
$$D_3=\frac{C_1C_2C_3}{k_2(G_{13}G_{23}+G_{12}G_{13}+G_{12}G_{23})}\quad(k_1=0\text{ and }k_3=0)\tag{10}$$

Except for slight changes in the coefficients, exactly the same equation results should the conduction effect be neglected in carriers 1 and 2 ($k_1 = 0$ and $k_2 = 0$) or in carriers 2 and 3 ($k_2 = 0$ and $k_3 = 0$):

$$D_{21}=\frac{C_1(G_{12}+G_{23})+C_2(G_{12}+G_{13})}{G_{13}G_{23}+G_{12}G_{13}+G_{12}G_{23}},\quad D_{22}=\frac{C_1C_2}{G_{13}G_{23}+G_{12}G_{13}+G_{12}G_{23}},$$
$$D_1=\frac{C_1+C_2+C_3}{k_3},\quad D_2=\frac{C_1C_2(G_{13}+G_{23})+C_1C_3(G_{12}+G_{23})+C_2C_3(G_{12}+G_{13})}{k_3(G_{13}G_{23}+G_{12}G_{13}+G_{12}G_{23})},$$
$$D_3=\frac{C_1C_2C_3}{k_3(G_{13}G_{23}+G_{12}G_{13}+G_{12}G_{23})}\quad(k_1=0\text{ and }k_2=0);$$
$$D_{21}=\frac{C_2(G_{13}+G_{23})+C_3(G_{12}+G_{23})}{G_{13}G_{23}+G_{12}G_{13}+G_{12}G_{23}},\quad D_{22}=\frac{C_2C_3}{G_{13}G_{23}+G_{12}G_{13}+G_{12}G_{23}},$$
$$D_1=\frac{C_1+C_2+C_3}{k_1},\quad D_2=\frac{C_1C_2(G_{13}+G_{23})+C_1C_3(G_{12}+G_{23})+C_2C_3(G_{12}+G_{13})}{k_1(G_{13}G_{23}+G_{12}G_{13}+G_{12}G_{23})},$$
$$D_3=\frac{C_1C_2C_3}{k_1(G_{13}G_{23}+G_{12}G_{13}+G_{12}G_{23})}\quad(k_2=0\text{ and }k_3=0).\tag{11}$$

The corresponding equations for T_1 and T_3 in each case, once again, remain exactly the same due to symmetry of energy exchange among three carriers. The mixed-derivative terms, $\partial^3T/\partial t\partial x^2$ and $\partial^4T/\partial t^2\partial x^2$ on the left-hand side and the wave ($\partial^2T/\partial t^2$) and jerk ($\partial^3T/\partial t^3$) terms on the right-hand side of Eq. (10), therefore, are common, which are the salient features characterizing nonequilibrium heat transport in the three-carrier system.

In passing, note that Eq. (1), including the special case of $N = 3$ in Eq. (4), could be viewed as a multi-step model since it is generalized from the two-step model for the case of two carriers (Eq. (2)). For problems involving known heating in one carrier, such as heated wicks in heat pipes that are cooled by the liquid and vapor phases, the energy generation term needs to be incorporated correspondingly in Eq. (4). For laser processing of materials involving multi-carriers, such as removal of burned skins by femtosecond lasers, a generic form describing the energy absorption rates in each carrier would work the best for a universal treatment. Different heating rates involved in each carrier are implemented in Eq. (4), with different heating rates adjusted through the use of different heating intensity in each carrier. Effect of volumetric heating will give rise to apparent heating in addition to the real heat source applied to the carriers [6], with all terms remaining the same as those in Eq. (10). Effect of volumetric heating, in other words, will not alter the characteristics of the energy equation, which are dictated by the derivatives of the highest orders in the energy equation. Such an effect has been excluded in this work in order for a better focus on the thermalization and relaxation behaviors without unnecessary complications from the heat source term.

3. Nonlinear behavior of thermal lagging

The dual-phase-lag model has been shown admissible within the frameworks of nonequilibrium irreversible thermodynamics [6,13], Boltzmann transport equation [14], and Galilean invariance principle in relativity [15]. The mixed derivate term in Eq. (10), $\partial^3T/\partial t\partial x^2$, and the wave ($\partial^2T/\partial t^2$) and jerk ($\partial^3T/\partial t^3$) terms have already been captured in the framework of thermal lagging accounting for the liner effects of τ_T and τ_q as well as the effect of τ_q^2 [5,6]. The mixed derivate term ($\partial^3T/\partial t\partial x^2$) effectively destroys the sharp wavefront introduced by the wave effect ($\partial^2T/\partial t^2$) in heat propagation, rendering a response of high-order diffusion whose temperature may be several times higher than that predicted by classical Fourier diffusion. Effect of τ_q^2 further introduces the jerk term ($\partial^3T/\partial t^3$) in the energy equation, bringing back thermal waves that may propagate many times faster than the classical Cattaneo–Vernotte (*CV*) thermal wave. Entering the arena of microscale heat transfer, in other words, there exists an alternating sequence of diffusion and thermal waves, as a result of shortening the response time, which can not be covered by either classical Fourier diffusion or *CV*-wave alone [6].

There exists a fourth-order, mixed-derivative term in Eq. (10), $\partial^4T/\partial t^2\partial x^2$, which has never appeared in the development of the dual-phase-lag (DPL) model. To understand its physical significance, we expand the constitutive relation with general delays by retaining the second-order effects in τ_T and τ_q:

$$\begin{aligned}\mathbf{q}(\mathbf{x},t+\tau_q)&=-k\nabla T(\mathbf{x},t+\tau_T)\\&\Rightarrow\mathbf{q}(\mathbf{x},t)+\tau_q\frac{\partial\mathbf{q}}{\partial t}(\mathbf{x},t)+\frac{\tau_q^2}{2}\frac{\partial^2\mathbf{q}}{\partial t^2}(\mathbf{x},t)\\&\cong-k\left[\nabla T(\mathbf{x},t)+\tau_T\frac{\partial}{\partial t}\nabla T(\mathbf{x},t)+\frac{\tau_T^2}{2}\frac{\partial^2}{\partial t^2}\nabla T(\mathbf{x},t)\right]\end{aligned}\tag{12}$$

The phase lags (both τ_T and τ_q), in other words, are assumed small in comparison with the process time (t) such that the third-order terms and higher (in τ_T and τ_q) are negligible. Note also that all quantities in Eq. (12) now occur *at the same instant of time* after the Taylor series expansion. Eliminating the heat flux vector from the energy equation,

$$C\frac{\partial T}{\partial t}(\mathbf{x},t)=-\nabla\cdot\mathbf{q}(\mathbf{x},t),\tag{13}$$

by first taking divergence over Eq. (12) and then substituting Eq. (13) into the result, the energy equation expressed in terms of temperature reads

$$\nabla^2T+\tau_T\frac{\partial}{\partial t}(\nabla^2T)+\frac{\tau_T^2}{2}\frac{\partial^2}{\partial t^2}(\nabla^2T)=\frac{1}{\alpha}\frac{\partial T}{\partial t}+\frac{\tau_q}{\alpha}\frac{\partial^2T}{\partial t^2}+\frac{\tau_q^2}{2\alpha}\frac{\partial^3T}{\partial t^3}\tag{14}$$

In the one-dimensional case with ∇^2 replaced by $\partial^2/\partial x^2$, Eq. (14) is reduced to

$$\frac{\partial^2T}{\partial x^2}+\tau_T\frac{\partial^3T}{\partial t\partial x^2}+\frac{\tau_T^2}{2}\frac{\partial^4T}{\partial t^2\partial x^2}=\frac{1}{\alpha}\frac{\partial T}{\partial t}+\frac{\tau_q}{\alpha}\frac{\partial^2T}{\partial t^2}+\frac{\tau_q^2}{2\alpha}\frac{\partial^3T}{\partial t^3},\tag{15}$$

which has exactly the same form as Eq. (10) for the three-carrier system, with T representing T_1, T_2, or T_3 in accordance with the coefficients Ds defined in Eqs. (10) and (11). While the linear effects of τ_T and τ_q contribute to the mixed-derivative ($\partial^3T/\partial t\partial x^2$) and the wave ($\partial^2T/\partial t^2$) terms, the nonlinear effects of τ_T^2 and τ_q^2 contribute to the jerk term ($\partial^3T/\partial t^3$) and the forth-order, mixed-derivative term ($\partial^4T/\partial t^2\partial x^2$). Complicated energy exchanges among the three energy carriers, obviously, have been nicely lumped into the linear and second-order effects of τ_T and τ_q.

Identical form of Eqs. (10) and (15) facilitates determination of the values of α, τ_T, and τ_q. In the case of $k_1 = 0$ and $k_3 = 0$, direct comparisons of the coefficients of the diffusion term ($\partial T/\partial t$, for α), the mixed-derivate term ($\partial^3T/\partial t\partial x^2$, for τ_T), and the wave term ($\partial^2T/\partial t^2$, for τ_q) give

$$\alpha=\frac{k_2}{C_1+C_2+C_3},\quad\tau_T=\frac{C_1(G_{13}+G_{23})+C_3(G_{12}+G_{13})}{G_{13}G_{23}+G_{12}G_{13}+G_{12}G_{23}}\sim\left[\frac{CG}{G^2}\right]\sim O\left[\frac{C}{G}\right]$$
$$\tau_q=\frac{C_1C_2(G_{13}+G_{23})+C_1C_3(G_{12}+G_{23})+C_2C_3(G_{12}+G_{13})}{(C_1+C_2+C_3)(G_{13}G_{23}+G_{12}G_{13}+G_{12}G_{23})}\sim\left[\frac{C^2G}{CG^2}\right]\sim O\left[\frac{C}{G}\right]\tag{16}$$

Estimated from the order of magnitudes, it can readily be seen that τ_T and τ_q are of the order of (C/G). The coefficients of τ_T^2 and τ_q^2, from the fourth-order, mixed-derivative term $(\partial^4 T/\partial t^2\partial x^2)$ and the jerk term $(\partial^3 T/\partial t^3)$ in Eqs. (10) and (15), result in

$$\tau_T^2=\frac{2C_1C_3}{G_{13}G_{23}+G_{12}G_{13}+G_{12}G_{23}}\sim\left[\frac{C^2}{G^2}\right]\sim O\left(\frac{C}{G}\right)^2$$
$$\tau_q^2=\frac{2C_1C_2C_3}{(C_1+C_2+C_3)(G_{13}G_{23}+G_{12}G_{13}+G_{12}G_{23})}\sim\left[\frac{C^3}{CG^2}\right]\sim O\left(\frac{C}{G}\right)^2 \tag{17}$$

Eq. (17) indicates that τ_T^2 and τ_q^2 are indeed of the order of $(C/G)^2$. With τ_T and τ_q shown in Eq. (16), in other words, the fourth-order, mixed-derivative term $(\partial^4 T/\partial t^2\partial x^2)$ and the jerk term $(\partial^3 T/\partial t^3)$ are indeed their second-order effects.

4. Numerical example

Even though the various orders of τ_T and τ_q have been mathematically incorporated in the general framework of thermal lagging [6], physically, this is the first time that the τ_T^2-effect is shown to exit in a physical system. Presence of the new mixed-derivative term, $\partial^4 T/\partial t^2\partial x^2$, in the heat equation necessitates a detailed analysis for understanding its effects on the nonequilibrium temperature with lagging behavior.

The problem that is able to reveal all fundamental behaviors of thermal lagging with minimal mathematical complication may be a semi-infinite solid whose initial temperature is kept uniform throughout, at T_0, and is disturbed from a stationary state:

$$T=T_0,\quad \frac{\partial T}{\partial t}=0,\quad \text{and}\quad \frac{\partial^2 T}{\partial t^2}=0\quad \text{as}\quad t=0 \tag{18}$$

Note that three initial conditions are needed since Eq. (15) involves the third-order derivative with respect to time, the jerk term resulting from the τ_q^2-effect. Temperature at the surface $x = 0$ is suddenly raised to T_w, whereas the thermal field remains undisturbed at a distance sufficiently far away from the heated boundary:

$$T=T_w\quad \text{at}\quad x=0,\quad T\to T_0\quad \text{as}\quad x\to\infty \tag{19}$$

Aiming at nonequilibrium heating during the early-time transient with $t\sim\tau_q$, we introduce the following nondimensional variables:

$$\xi=\frac{x}{\sqrt{\alpha\tau_q}},\quad \beta=\frac{t}{\tau_q},\quad \theta=\frac{T-T_0}{T_w-T_0},\quad z=\frac{\tau_T}{\tau_q}. \tag{20}$$

Eqs. (15), (18), and (19) become

$$\frac{\partial^2\theta}{\partial\xi^2}+z\frac{\partial^3\theta}{\partial\beta\partial\xi^2}+\frac{z^2}{2}\frac{\partial^4\theta}{\partial\beta^2\partial\xi^2}=\frac{\partial\theta}{\partial\beta}+\frac{\partial^2\theta}{\partial\beta^2}+\frac{1}{2}\frac{\partial^3\theta}{\partial\beta^3};$$
$$\theta=0,\quad \frac{\partial\theta}{\partial\beta}=0,\quad \text{and}\quad \frac{\partial^2\theta}{\partial\beta^2}=0\quad \text{as}\quad \beta=0; \tag{21}$$
$$\theta=1\quad \text{at}\quad \xi=0,\quad \theta\to 0\quad \text{as}\quad \xi\to\infty.$$

The Laplace transform solution to Eq. (21) can readily be obtained

$$\bar\theta(\xi;p)=\frac{\exp\left[-\sqrt{\frac{p(2+2p+p^2)}{2+2(pz)+(pz)^2}}\xi\right]}{p} \tag{22}$$

Resulting from the infinite physical domain and simple initial/boundary conditions, the temperature response depends on the ratio of τ_T to τ_q, $z = \tau_T/\tau_q$, rather than the individual values of τ_T and τ_q. In terms of volumetric heat capacities and energy coupling factors of the three energy carriers, referring to Eq. (16),

$$z=\frac{\left(1+\frac{C_2}{C_1}+\frac{C_3}{C_1}\right)\left[\left(\frac{C_3}{C_1}\right)\left(1+\frac{G_{13}}{G_{12}}\right)+\left(\frac{G_{13}}{G_{12}}+\frac{G_{23}}{G_{12}}\right)\right]}{\left(\frac{C_2}{C_1}\right)\left(\frac{C_3}{C_1}\right)\left(1+\frac{G_{13}}{G_{12}}\right)+\left(\frac{C_3}{C_1}\right)\left(1+\frac{G_{23}}{G_{12}}\right)+\left(\frac{C_2}{C_1}\right)\left(\frac{G_{13}}{G_{12}}+\frac{G_{23}}{G_{12}}\right)} \tag{23}$$

The value of z, clearly, depends on two heat-capacity ratios and two energy-coupling-factor ratios. Laplace inversion of Eq. (22) can be performed by the Riemann sum approximation for the Bromwich contour integral [5,6,16]:

$$\theta(\xi,\beta)\cong\frac{e^{\gamma\beta}}{\beta}\left[\frac{1}{2}\bar\theta(\xi;p=\gamma)+\mathrm{Re}\sum_{n=1}^{N}\bar\theta(\xi;p=\gamma+\frac{in\pi}{\beta})(-1)^n\right] \tag{24}$$

where the value of γ is chosen to be $4.7/\beta$ for faster convergence of the numerical summation.

In presence of thermal lagging, the flux-precedence type of heat flow ($\tau_q < \tau_T$ or $z > 1$) distinguishes itself from the gradient-precedence type of heat flow ($\tau_T < \tau_q$ or $z < 1$). The case of $z = 1$, or $\tau_T = \tau_q$, implies a simultaneous response between the heat flux vector and the temperature gradient, for which Eq. (15) is reduced to the classical diffusion equation employing the Fourier's law. Since the energy coupling factors are positive definite, namely $G_{12} > 0$, $G_{23} > 0$, and $G_{13} > 0$, it is important to note that the z-value shown by Eq. (23) always renders a *flux*-precedence type of heat flow because z is always greater than unity ($z > 1$). This can be seen by the difference between the numerator and the denominator of Eq. (23):

$$\left\{\left(1+\frac{C_2}{C_1}+\frac{C_3}{C_1}\right)\left[\left(\frac{C_3}{C_1}\right)\left(1+\frac{G_{13}}{G_{12}}\right)+\left(\frac{G_{13}}{G_{12}}+\frac{G_{23}}{G_{12}}\right)\right]\right\}$$
$$-\left\{\left(\frac{C_2}{C_1}\right)\left(\frac{C_3}{C_1}\right)\left(1+\frac{G_{13}}{G_{12}}\right)+\left(\frac{C_3}{C_1}\right)\left(1+\frac{G_{23}}{G_{12}}\right)+\left(\frac{C_2}{C_1}\right)\left(\frac{G_{13}}{G_{12}}+\frac{G_{23}}{G_{12}}\right)\right\}$$
$$=\left(\frac{G_{23}}{G_{12}}\right)+\left(\frac{C_3}{C_1}\right)^2+\left(\frac{G_{13}}{G_{12}}\right)\left(1+\frac{C_3}{C_1}\right)^2>0. \tag{25}$$

In studying the lagging temperature represented by Eqs. (22) and (24), therefore, we will restrict our studies to the case of $z > 1$.

The z-surface shown by Eq. (23) is characterized by four parameters: (G_{13}/G_{12}), (G_{23}/G_{12}), (C_2/C_1), and (C_3/C_1). Fig. 2 shows the variations of z with respect to (G_{13}/G_{12}) and (G_{23}/G_{12}) for $(C_2/C_1) < 1$ and $(C_3/C_1) > 1$ (Fig. 2(a)) and $(C_2/C_1) > 1$ and $(C_3/C_1) < 1$ (Fig. 2(b)), as well as the variations with respect to (C_2/C_1) and (C_3/C_1) for $(G_{13}/G_{12}) < 1$ and $(G_{23}/G_{12}) > 1$ (Fig. 2(c)) and $(G_{13}/G_{12}) > 1$ and $(G_{23}/G_{12}) < 1$ (Fig. 2(d)). The value of z increases (decreases) as the value of G_{13}/G_{12} (G_{23}/G_{12}) increases (decreases), as shown in Fig. 2(a). As the value of G_{13}/G_{12} (G_{23}/G_{12}) approaches infinity, however, the value of z approaches the limit of 31 (1.19231). A similar trend can be observed in Fig. 2(b), where the value of z increases with both values of (G_{13}/G_{12}) and (G_{23}/G_{12}). The limiting values of z in this case are 1.24 (1.19231) as the value of G_{13}/G_{12} (G_{23}/G_{12}) approaches infinity. Fig. 2(c) shows that the value of z decreases as the value of (C_2/C_1) increases. A stationary value of z in (C_3/C_1), however, exists in the regime with $(C_2/C_1) < 1$.

Eqs. (15) and (21), and hence the solution shown by Eq. (22), recover the cases of Fourier diffusion ($\tau_T = \tau_q$ or $z = 1$), *CV*-wave (τ_q-effect alone), linearized DPL (effects of both τ_T and τ_q), and *T*-wave (effects of τ_T, τ_q, and τ_q^2) as the high-order derivatives describing the high-rate effects are gradually extracted in correspondence. From low-order to high-order models describing the various effects of τ_T and τ_q that are active/diminishing in different domains of time [17], the corresponding solutions of $(\bar\xi;p)$ are

$$\text{Fourier diffusion}:\ \frac{\partial^2\theta}{\partial\xi^2}=\frac{\partial\theta}{\partial\beta}\ \Rightarrow\ \bar\theta(\xi;p)=\frac{\exp\left[-\sqrt{p}\xi\right]}{p},$$
$$\text{CV-wave}:\ \frac{\partial^2\theta}{\partial\xi^2}=\frac{\partial\theta}{\partial\beta}+\frac{\partial^2\theta}{\partial\beta^2}\ \Rightarrow\ \bar\theta(\xi;p)=\frac{\exp\left[-\sqrt{p(1+p)}\xi\right]}{p},$$
$$\text{Linearized DPL}:\ \frac{\partial^2\theta}{\partial\xi^2}+z\frac{\partial^3\theta}{\partial\beta\partial\xi^2}=\frac{\partial\theta}{\partial\beta}+\frac{\partial^2\theta}{\partial\beta^2}\Rightarrow\bar\theta(\xi;p)=\frac{\exp\left[-\sqrt{\frac{p(1+p)}{1+pz}}\xi\right]}{p},$$
$$\text{T-wave}:\ \frac{\partial^2\theta}{\partial\xi^2}+z\frac{\partial^3\theta}{\partial\beta\partial\xi^2}=\frac{\partial\theta}{\partial\beta}+\frac{\partial^2\theta}{\partial\beta^2}+\frac{1}{2}\frac{\partial^3\theta}{\partial\beta^3}\Rightarrow\bar\theta(\xi;p)=\frac{\exp\left[-\sqrt{\frac{p(2+2p+p^2)}{2(1+pz)}}\xi\right]}{p}. \tag{26}$$

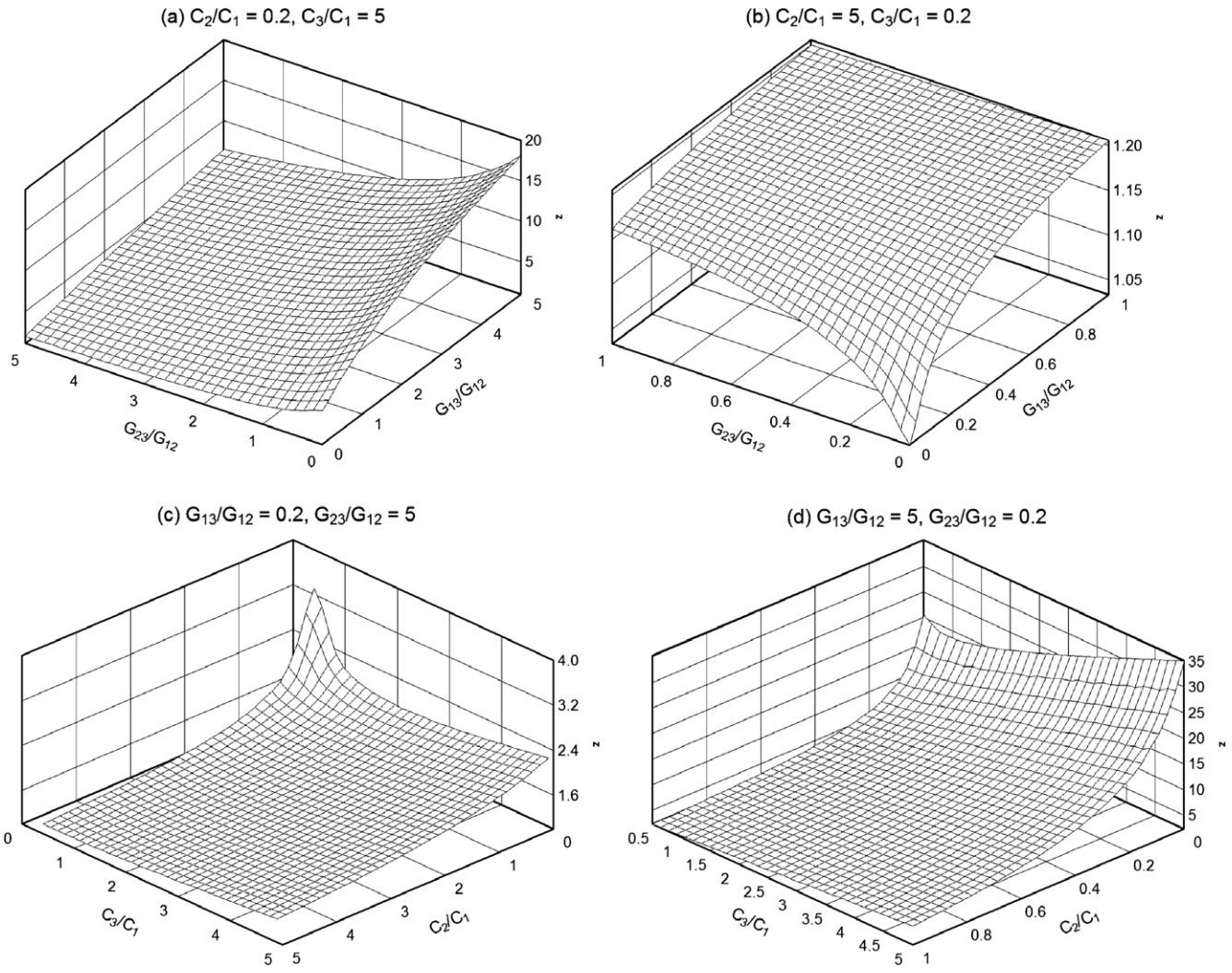

Fig. 2. Variations of z as a function of G_{13}/G_{12} and G_{23}/G_{12} for (a) $C_2/C_1 = 0.2$ and $C_3/C_1 = 5$, (b) $C_2/C_1 = 5$ and $C_3/C_1 = 0.2$, and that of C_2/C_1 and C_3/C_1 for (c) $G_{13}/G_{12} = 0.2$ and $G_{23}/G_{12} = 5$, and (d) $G_{13}/G_{12} = 5$ and $G_{23}/G_{12} = 0.2$.

With such high-rate effects covered in the same framework of thermal lagging, DPL is able to reveal the ways in which a certain effect evolves/reduces to another as transient time continuously shortened/lengthened. These expressions are used in Eq. (24) when compared with the expression containing the τ_T^2 effect shown by Eq. (22).

Fig. 3 shows the temperature distributions during the ultrafast transient predicted by the various model, at a representative instant of time of $\beta = 1$, or $t = \tau_q$. The value of z is taken to be five, $\tau_T = 5\tau_q$, as compared to $\tau_T \cong 0\tau_q$ for most metals. In the heat affected zone where a significant temperature rise prevails, the temperature level increases with the degrees of thermal lagging measured by the orders of τ_T and τ_q. The linear DPL model with τ_T- and τ_q-effect, for example, results in higher temperatures than those predicted by Fourier's law (no lagging) and *CV*-wave model (τ_q-effect only). As the nonlinear effects of τ_T^2 and τ_q^2 gradually enter the Taylor series expansion shown in Eq. (12), showing that the transient time (t) is of the same orders of magnitude as τ_T^2 and τ_q^2 in the physical response, the *T*-wave (containing effects of τ_T, τ_q, and τ_q^2) and the DPL model with additional effect of τ_T^2 further elevate temperatures in the heat affected zone. A sharp wavefront, which separates the heat affected zone from the thermally undisturbed zone in the physical domain, is attributed to the phase lag of the heat flux vector, τ_q. In the presence of the linear effect of τ_q, the classical *CV*-wave, the wavefront is located at $x = \sqrt{\alpha/\tau_q}\, t$ or $\xi = \beta$ according to the nondimensional scheme introduced in Eq. (20). In the case of *T*-wave where the effect of τ_q^2 is further incorporated during the ultrafast transient, location of the wavefront is at $x = \sqrt{(2\alpha\tau_T)/\tau_q}\, t$ or $\xi = \sqrt{2z}\,\beta$. As $\beta = 1$ ($t = \tau_q$) and $z = 5$, locations of the thermal wavefront are at $\xi = 1$ (*CV*-wave) and $\xi = \sqrt{10} \cong 3.16$ (*T*-wave), respectively. As shown in Fig. 3, the method of Riemann sum approximation for the Laplace inversion captures these locations very well.

Tangling of the response curves of *T*-wave (with τ_q^2-effect) and DPL (with the additional τ_T^2-effect) models shown in Fig. 3 results from the chosen value of z. As the value of z increases, exemplified by $z = 10$ in Fig. 4, the two curves separate with a wider margin, and the τ_T^2-effect in thermal lagging clearly yields a higher temperature than the τ_q^2-effect alone (*T*-wave). The location of the wavefront is advanced to $\xi_T = \sqrt{2z}\beta \cong 4.47$ in the case of $z = 10$, which is again well captured by the method of the Riemann sum approximation.

Lagging behavior is a salient feature during the ultrafast transient with t comparable to τ_T and τ_q. As time lengthens, as shown by $\beta = 20$ in Fig. 5, thermal wavefronts (*CV*- and *T*-wave) disappear and all responses start to collapse onto the same curve. At $z = 5$, the response curve becomes indistinguishable as β increases over 30.

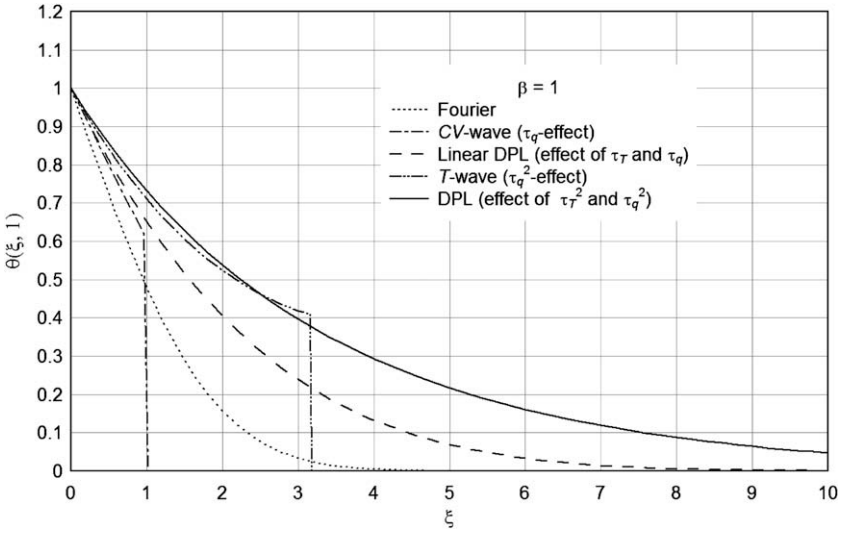

Fig. 3. Comparisons of Fourier diffusion ($\tau_T = \tau_q$), *CV*-wave (effect of τ_q), linear DPL (effect of τ_T and τ_q), *T*-wave (τ_q^2-effect), and DPL (effect of τ_T^2 and τ_q^2).

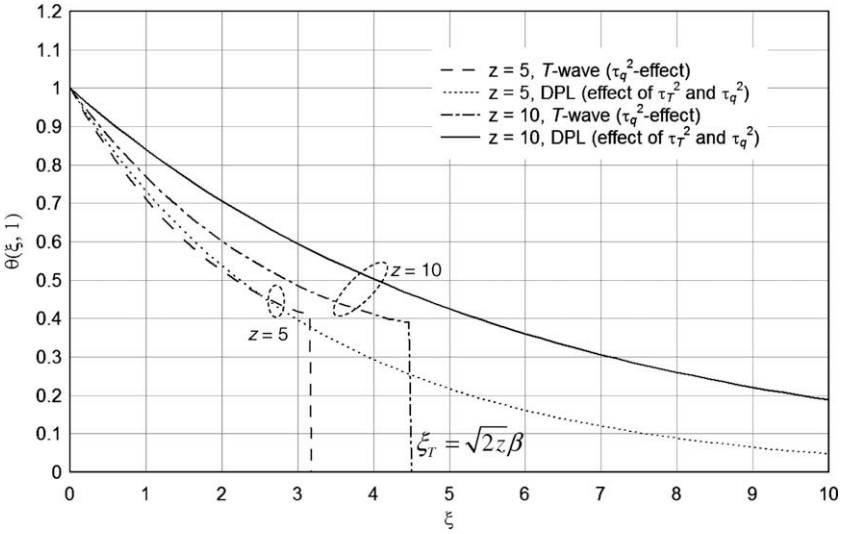

Fig. 4. Effect of $z(\tau_T/\tau_q)$ on *T*-wave (effect of τ_q^2) and DPL (effect of both τ_T^2 and τ_q^2): $\beta = 1$.

5. Conclusion

The microscopic two-step model has been generalized to describe nonequilibrium heating in systems containing multiple energy carriers. The thermalization time (τ_T) and relaxation time (τ_q) are extracted from the resulting energy equation, showing that the increasing number of energy carriers result in high-order effects in τ_T and τ_q. For the case of three carriers, for instance, thermal lagging with second-order effects of τ_T and τ_q will be present during the nonequilibrium response. More generally, the method of deduction has shown that nonequilibrium heating in a system with *N* carriers will result in thermal lagging of the order up to $\tau_T^{(N-1)}$ and $\tau_q^{(N-1)}$. Within the context of energy exchange proportional to the temperature difference, as that described in the two-step model, in other words, the phase lags (time constants) characterizing the lagging behavior remain to be τ_T and τ_q, regardless of the number of energy carriers involved in the system.

It is essential to continue identifying physical systems that may display a combined behavior of ultrafast thermalization and relaxation as the various orders in τ_T and τ_q are introduced in the general framework of thermal lagging. The τ_T^2 and τ_q^2 effects resulting from the case of three energy carriers, as explored in this work, should shed light on the fundamental understandings of nonequilibrium heating in more complicated systems, such as in multi-constituent composites, interfacial heat transfer, wicked heat pipes (for high heat removal) and/or biomedical/biological tissues when processed by ultrafast lasers. As compared to the *T*-wave with the τ_q^2-effect alone, the second-order effect of in thermalization (τ_T) further elevates the temperature level, now becoming 3–4 times higher than that predicted by Fourier diffusion without accounting for the effect of thermal lagging. The *T*-wave (containing the τ_q^2-effect) propagates faster than the conventional *CV*-wave (effect of τ_q). In presence of the additional τ_T^2-effect, however, the wavefront is destroyed and heat propagation by high-order diffusion is recovered. In absence of a heat source, the lagging behavior is characterized by the ratio of τ_T to τ_q, which has been expressed in terms of two heat-capacity and two energy-coupling-factor ratios for the three-carrier system. The ratio of τ_T to τ_q is shown to be greater than unity, rendering a flux-precedence type of heat flow ($\tau_q < \tau_T$) in physically

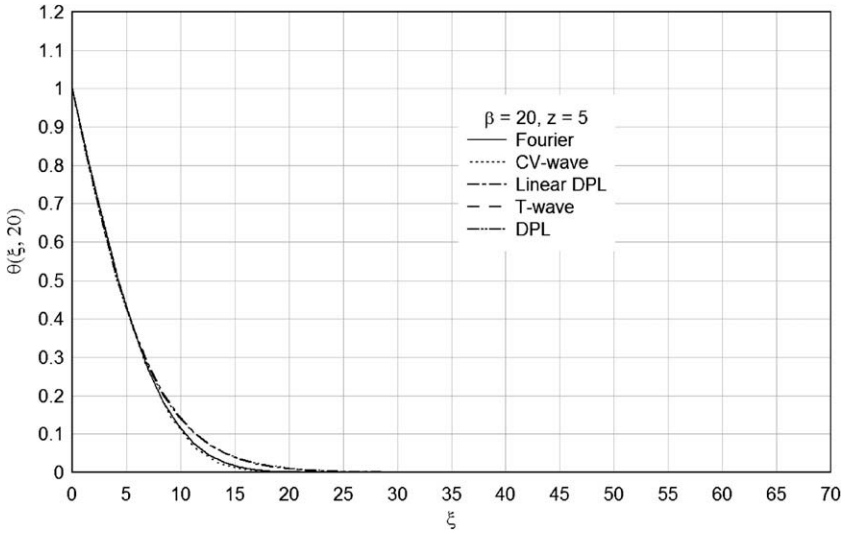

Fig. 5. Diminution of wavefronts (for *CV*- and *T*-wave) and coalesce of all models at long times: $\beta = 20$.

admissible systems where both heat capacities and energy coupling factors are positive definite.

Real physical systems, particularly the microscopic biological and biomedical systems, may involve a number of species/carriers in transporting heat. Energy absorption of ultrafast lasers by hard/soft tissues through complicated body fluids, where another set of energy carriers may also be involved, for example, may involve more than three carriers in accomplishing the entire process of treatments by ultrafast lasers. As the number of energy carriers continuously increases, following the initial effort as presented in this work, an important task to be accomplished in the next phase will be on the rise of the orders of τ_T and τ_q in thermal lagging as a result of increasing the numbers of energy carriers. The resulting physical response will be complicated, evidenced by the various mixed- and time-derivatives in the energy equation describing thermal lagging. We will leave this subject in future communications.

References

[1] M.I. Kaganov, I.M. Lifshitz, M.V. Tanatarov, Relaxation between electrons and crystalline lattices, Sov. Phys. JETP 4 (1957) 173–178.
[2] S.I. Anisimov, B.L. Kapeliovich, T.L. Perel'man, Electron emission from metal surfaces exposed to ultra-short laser pulses, Sov. Phys. JETP 39 (1974) 375–377.
[3] T.Q. Qiu, C.L. Tien, Short-pulse laser heating on metals, Int. J. Heat Mass Transfer 35 (1992) 719–726.
[4] T.Q. Qiu, C.L. Tien, Heat transfer mechanisms during short-pulse laser heating of metals, ASME J. Heat transfer 115 (1993) 835–841.
[5] D.Y. Tzou, A unified field approach for heat conduction from micro- to macroscales, ASME J. Heat Transfer 117 (1995) 8–16.
[6] D.Y. Tzou, Macro- to Microscale Heat Transfer: The Lagging Behavior, Taylor & Francis, Washington, DC, 1997.
[7] W.J. Minkowycz, A. Haji-Sheikh, K. Vafai, On departure from local thermal equilibrium in porous media due to a rapidly changing heat source: the Sparrow number, Int. J. Heat Mass Transfer 42 (1999) 3373–3385.
[8] D.Y. Tzou, J.K. Chen, Thermal lagging in random media, AIAA J. Thermophys. Heat Transfer 12 (1998) 567–574.
[9] A. Faghri, Y. Zhang, Transport Phenomena in Multiphase Systems, Elsevier, Amsterdam, 2006.
[10] F. Dausinger, F. Lichtner, H. Lubatschowski (Eds.), Femtosecond Technology for Technical and Medical Applications, Springer, Berlin, 2004.
[11] W. Dai, F. Zhu, D.Y. Tzou, An unconditionally stable finite difference scheme for thermal analysis in a multi-carrier system, Int. J. Therm. Sci. (submitted for publication).
[12] L.Q. Wang, X.H. Wei, Equivalence between dual-phase-lagging and two-phase system heat conduction processes, Int. J. Heat Mass Transfer 51 (2008) 1751–1756.
[13] M.A. Al-Nimr, M. Naji, V.S. Arpaci, Nonequilibrium entropy production under the effect of the dual-phase-lag heat conduction model, ASME J. Heat Transfer 122 (2000) 217–223.
[14] M. Xu, L. Wang, Dual-phase-lagging heat conduction based on Boltzmann transport equation, Int. J. Heat Mass Transfer 48 (2005) 5616–5624.
[15] L. Cheng, M. Xu, L. Wang, From Boltzmann transport equation to single-phase-lagging heat conduction, Int. J. Heat Mass Transfer (submitted for publication).
[16] D.Y. Tzou, Computational techniques for microscale heat transfer, in: W.J. Minkowycz, E.M. Sparrow, J.Y. Murthy (Eds.), Handbook of Numerical Heat Transfer, second ed., Wiley, New Jersey, 2006, pp. 623–657 (Chapter 20).
[17] D.Y. Tzou, Heat propagation: duality of diffusion and waves, panel session 3–4 on dual-phase-lagging heat conduction, ASME Micro/Nanoscale Heat Transfer International Conference, Tainan, Taiwan, January 6–9, 2008.